Orbital: The Electronic Journal of Chemistry
journal homepage: www.orbital.ufms.br
e-ISSN 1984-6428

| Vol 10 | | No. 5 | | April-June 2018 |

FULL PAPER

Zirconium Oxide and Iron Zirconate Obtained from Citrus Pectin and Nitrates Applied in the Photo-fenton-like Process

Cristiane Antoniazzi, Eryza Guimarães de Castro[a], and Fauze Jacó Anaissi*

[a]Universidade Estadual do Centro-Oeste, Setor de Ciências Exatas e da Terra, Departamento de Química, Laboratório de Materiais e Compostos Inorgânicos, Rua Simeão Varela de Sá, 03, CEP: 85040-080, Guarapuava, PR, Brazil.

Article history: Received: 30 March 2017; revised: 18 May 2018; accepted: 09 June 2018. Available online: 30 June 2018. DOI: http://dx.doi.org/10.17807/orbital.v10i5.980

Abstract:

This paper describes the synthesis and characterization of zirconium oxide (ZrO_2) and of the mixed oxide of iron (iron zirconate), obtained by gelification (80 °C) and calcination (600 °C) of citrus pectin and inorganic nitrates. Thermal analysis demonstrated the presence of organic matter in the solid after calcination, indicating that pectin was strongly coordinated to the oxide phases. The X-ray diffractogram for zirconate, do not show peaks associated with the iron oxides phases, indicating that the zirconia matrix remained unchanged. Electronic spectra supported observations concerning the color of the solids, with bands assigned to d–d transitions of the iron ions. Both Raman spectra and X-ray diffractogram indicated the presence of the tetragonal phase of ZrO_2, and scanning electron microscopy images showed that the solids had similar and particulate morphologies. Finally, the test for dye degradation using iron zirconate proved efficient, with a degradation index greater than 90.3% after 60 min.

Keywords: citric pectin; degradation; iron-zirconate; photocatalysis; zirconium

1. Introduction

There has been a growing interest in zirconium oxide (ZrO_2), commonly known as zirconia, motivated by its good catalytic properties and wide range of applications, acting either as a matrix support or as a catalyst [1]. Interesting results have been reported in the literature for its pure and doped forms due to its high thermal stability and acid–base properties [1-3].

The development of methods to obtain zirconia is an important problem that deserves further investigation and improvement. Zirconia is polymorphic, and depending on the preparation method and calcination temperature, one of its phases forms preferentially. Thus, the amorphous, monoclinic, or tetragonal phases can form at 1170 °C, whereas the cubic form is only obtained at temperatures above 2680 °C [4]. The polymorphic nature of the oxide makes it useful in multiple industrial applications because each crystal phase has different properties. For instance, in the monoclinic form, ZrO_2 is more stable at ambient temperature and pressure [5], whereas the tetragonal form requires incorporation of other metal ions such as titanium, yttrium, nickel, sodium and boron or cerium to stabilize it [6-10].

A large variety of oxides are prepared with the focus on a specific synthesis route. ZrO_2 can be obtained by sol-gel, Pechini, and co-precipitation methods. Here, we present a method based on the use of citrus pectin as a non-conventional gelling precursor in the synthesis of oxides [11]. Citrus pectin is a natural polysaccharide [12] present in the cell walls of plants and fruits, and it is extracted mainly from citrus fruits and apples [13], where it is found in the form of pectinic acids. This form of pectin is widely used in the food industry as a gelling agent, as well as in supplements and vitamins [12-15].

There is currently great interest in the

*Corresponding author. E-mail: fjanaissi@gmail.com

development of materials that contribute to the well-being of people, materials such as those used in the treatment of industrial wastewaters. Moreover, the development of new materials also impacts technological and scientific advances. However, this development must be guided by the use of clean synthesis routes, cost control, and the minimization of waste products associated with their preparation.

The environmental pollution by toxic chemicals such as organic compounds and heavy metals is a serious problem [16]. Textile industry as one of important water consumers produces highly colored and complex wastewater [17]. Numerous researchers have evaluated the treatment of organic pollutants by so-called advanced oxidation processes (AOPs). Azo dyes and their derived products, commonly used in textile industry are largely employed, due to their higher performance when compared to other kinds of dye are usually characterized by the presence of azo chromophores (N≡N) or phthalocyanine chromophore (containing copper, nickel or other metals) and aromatic rings. These groups are considered toxic and mutagenic to living organism to present high pollution potential [18].

Advanced oxidation processes (AOPs) are methods based on the generation of hydroxyl radicals (•OH), which have a high oxidation power (E^o = 2.8 V vs. SHE), allowing for the degradation of organic compounds with great efficiency [19, 20]. An important AOP is the Fenton process, which relies on the production of hydroxyl radicals from hydrogen peroxide and ferrous salts in acid medium (Eq. 1). This reaction allows the efficient degradation of many pollutants in the treatment of water and wastewaters containing pharmaceuticals residues from the textile and paper industries [20].

$$Fe^{2+} + H_2O_2 \rightarrow Fe^{3+} + \bullet OH + OH^- \quad (1)$$

The process efficiency can be improved with the use of UV-B (280 to 320 nm), UV-A (320 to 400 nm), and VIS (400 to 800 nm) irradiation, in which case the process is called photo-Fenton (Eq. 2). The two reactions, Fenton and photo-Fenton occur simultaneously in the reaction medium, and because there is a pre-dominance of ferric ions, the pH of the solution must be less than four (pH < 4), to avoid precipitation of ferric oxyhydroxide [19, 20].

$$Fe^{3+} + H_2O_2 + hv\ (UV\ or\ Vis) \rightarrow Fe^{2+} + H^+ + \bullet OH \quad (2)$$

Therefore, in this study, zirconium oxide and the mixed oxide of iron were synthesized, and their thermal, structural, morphological, and spectroscopic properties were characterized using thermogravimetric-differential thermal analysis, X-ray diffraction, scanning electron microscopy, and electronic and Raman spectroscopy, respectively. Photocatalytic degradation tests on textile dye were also performed with the iron zirconate, the prepared oxides showed potential as alternative catalysts to TiO_2, a semiconductor widely used in heterogeneous photocatalytic processes [21]. In this paper, conducted the study to analyze the feasibility the system photo fenton-like for the degradation of azo dye, of Reactive Black 19. The ratio of parameters affecting the decolorization such as initial concentration of iron, H_2O_2 and initial pH value of dye solution were investigated.

2. Results and Discussion

The main advantage of the synthetic method used in this study is the ability to form precursors of inorganic structures at low temperatures (80 °C), making it a versatile and a simple manipulation method that allows one to predict the composition of the prepared oxides. Some preliminary tests were performed in order to determine the influence of factors such as the concentrations of citrus pectin and zirconium nitrate with and without agitation. The optimization of the synthesis conditions was important for improving the catalytic activity of the mixed oxide as compared with the individual oxide [22].

Thermal and structural behavior

Thermal analysis curves of precursors were obtained to define the decomposition stages and the phase transition temperature. The temperature was set to 600 °C for calcination at a rate of 10 °C min^{-1}. Above this temperature, no thermal events involving mass variation were observed.

Figure 1A shows the thermal curve of pectin, in which two exothermic events at 470 °C and 520 °C can be seen. These are assigned to the breakdown of the pectin chains, i.e., pectin's

depolymerization, associated with the decomposition and burning of the polymer. The corresponding curve of the zirconium nitrate is shown in Figure 1B, where the loss of mass in the 30 - 200 °C temperature range is associated with dehydration. The mass loss in the 200 - 400 °C range is associated with dehydration upon crystallization and with the sublimation of the nitrate ions. In the DTA curve, the event is associated with an exothermic peak at 470 °C, suggesting that there is a phase transition of ZrO_2 to the tetragonal phase [23].

As seen in Figure 1C, the precursor gel of $Zr_{(pec)}$ depicts some mass loss events in the 30 - 200 °C temperature range. The first process, up to 120 °C, is attributed to dehydration, accompanied by the endothermic peak in the DTA curve. A second process, above 120 °C, is associated with the decomposition of inorganic residues; it too is accompanied by an endothermic peak in the DTA curve. A mass decrease below 90% takes place at the end of the decomposition curve. The exothermic event in the 380 - 450 °C range is according to the literature, due to the initial formation of the tetragonal phase of zirconia, which in some cases may occur in this temperature range, significantly below the value of 1170 °C [23].

The thermal analysis curves of $Zr_{(pec)}$ (Figure 1D) and Fe_$Zr_{(pec)}$ (Figure 1E), both in powder form, are similar, with a total mass loss under 5%. This mass loss are due to dehydration (30 - 600 °C), whereas above 500 °C, these are associated with phase transitions such as oxide crystallization. For Fe_$Zr_{(pec)}$ above 600 °C, the formation of iron oxide takes place, involving a small loss of mass.

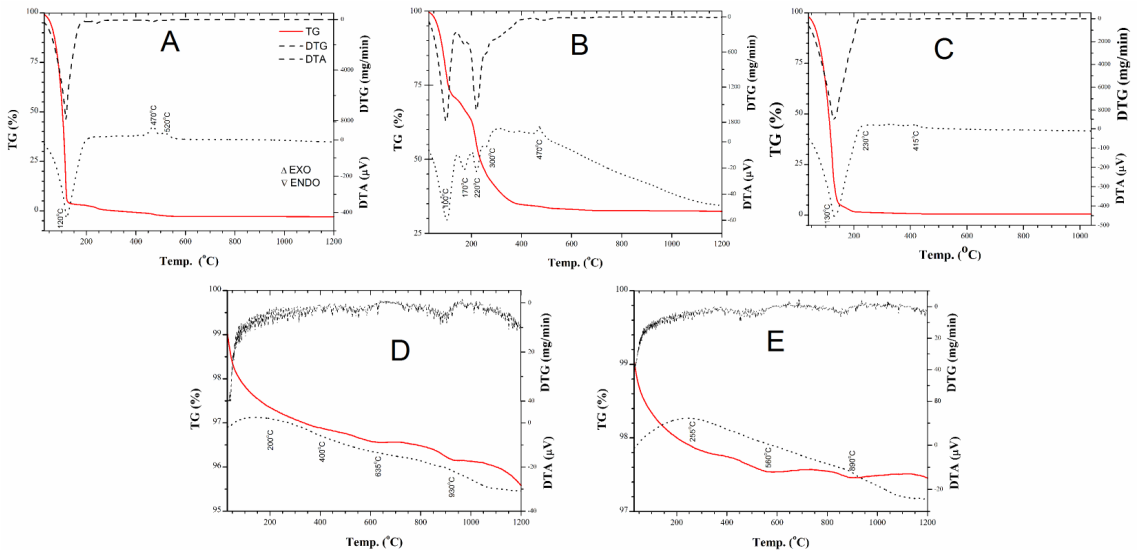


Figure 1. Simultaneous TG-DTG-DTA curves for: A) citrus pectin (pec); (B) zirconium nitrate; (C) gel precursor; (D) $Zr_{(pec)}$ and (E) Fe_$Zr_{(pec)}$.

The XRD patterns of the precursors are shown in Figure 2, where the anhydrous zirconium nitrate (Figure 2A) displays sharp peaks characteristic of crystalline materials. The calculations performed with the program Diffrac.Evaluation (Diffrac.EVA, Bruker) indicate a crystallinity value above 70%, whereas citrus pectin (Figure 2B) exhibits behavior typical of semicrystalline polymers with an amorphous halo. A mixture of phases was identified from the XRD pattern of the $Zr_{(pec)}$ [24] sample (Figure 2C). The phases corresponding to the cubic (PDF 0491642 and PDF 01071-4810) and the tetragonal (PDF 0727115) systems were identified according to the crystallographic charts. In some cases, the tetragonal phase of zirconia (t-ZrO_2) occurs through heating of the sample at a temperature of 450 °C. Stefanic and co-workers [25], using three different zirconium salts, concluded that the formation of t-ZrO_2 depends on the nature of the starting salt [25]. The formation of the tetragonal phase is due to hydration of the nitrate precursor, as complete loss of coordinated water does not occur at the calcination temperature. Diffraction peaks characteristic of the tetragonal phase at 2θ (hkl) values of 30.24 (101), 50.37 (112), and 60.10° (211) were

observed.

The XRD pattern of Fe_$Zr_{(pec)}$ (Figure 2D) is similar to that of $Zr_{(pec)}$ (Figure 2C), with just some minor differences in structure. The insertion of Fe^{3+} ions into the $Zr_{(pec)}$ matrix was not detected as a new phase be-cause the available concentration is considered low. Another important factor to consider is the size of the metal ions. When we compared the size of the ionic radii of Zr^{4+} (CN/r^{+}Å – 4/0.59 Å or 6/0.72 Å) and Fe^{3+} (CN/r^{+}Å – 4/0.49 Å or 6/0.55 Å), the Zr^{4+} ion was always bigger relative to the ligand number [26], indicating the ease with which iron was incorporated into the $Zr_{(pec)}$ matrix.

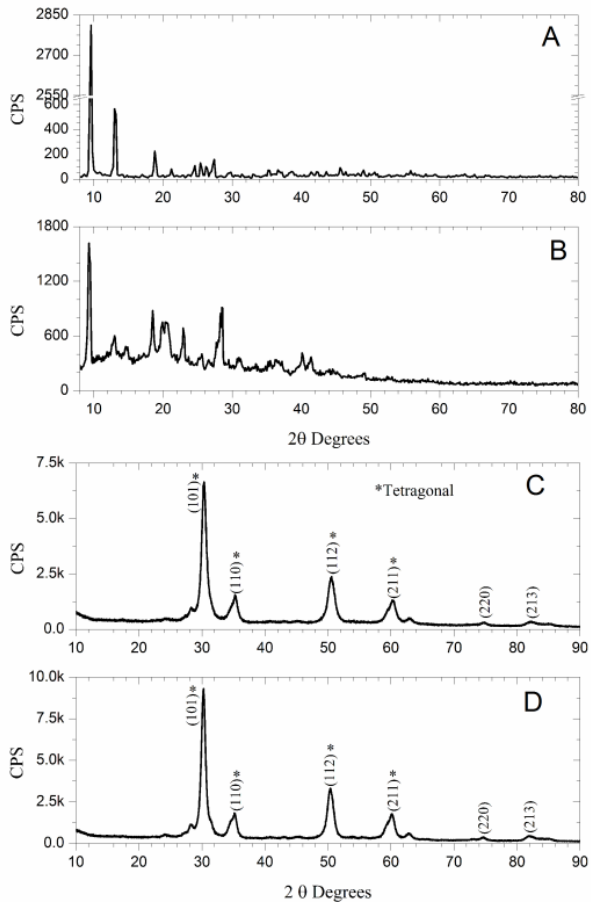


Figure 2. XRD profiles of the materials: (A) anhydrous zirconium nitrate; (B) citrus pectin (pec); (C) $Zr_{(pec)}$ and (D) Fe_$Zr_{(pec)}$.

UV-VIS and Raman spectroscopic behavior

The first striking feature of the materials is the color. The $Zr_{(pec)}$ matrix is white, whereas Fe_$Zr_{(pec)}$ is brown. As seen from the electronic spectra of the solids (Figure 3A), the $Zr_{(pec)}$ matrix (black line) shows no absorption bands characteristic of white solids, whereas the spectrum of Fe_$Zr_{(pec)}$ (red line) has a band at 485 nm assigned to the metal–oxygen bond Fe^{3+} ions in an octahedral environment [25]. The band gap (EBG) of Fe_$Zr_{(pec)}$ was calculated through the Tauc method [27] (Figure 3B). A value of 0.83 eV was found and compared to the literature value of 2.2 eV, enabling, therefore, its use in photo-Fenton processes for absorbing visible light.

The Raman spectrum of $Zr_{(pec)}$ (Figure 3C) is typical of the tetragonal phase. There have been reports in the literature where six characteristic bands with frequencies of 148, 263, 325, 472, 608, and 640 cm^{-1} were assigned to t-ZrO_2 [28]. In this case, the $Zr_{(pec)}$ matrix displays five of these bands (146, 265, 317, 471, and 642 cm^{-1}), indicating the formation of the tetragonal phase. For Fe_$Zr_{(pec)}$ (Figure 3C), the bands related to t-ZrO_2 undergo small displacements when compared to the $Zr_{(pec)}$ matrix (148, 266, 318, 464, and 638 cm^{-1}), showing an additional band at 715 cm^{-1}. In the literature, the band in the 720 cm^{-1} range is assigned to Fe–O vibrations of the akaganeite [29].

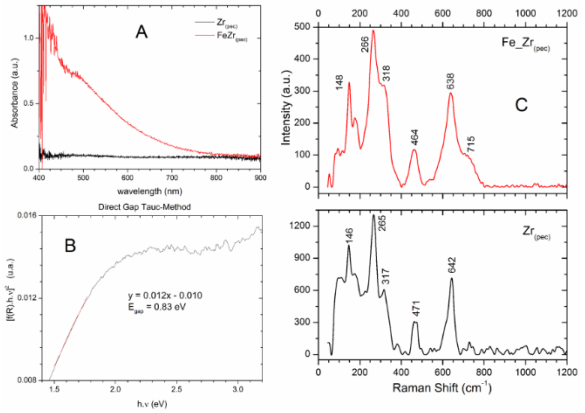


Figure 3. Diffuse reflectance electronic spectra (UV-Vis) for the materials (A) $Zr_{(pec)}$ – black line and Fe_$Zr_{(pec)}$ – red line. (B) Band gap energy (E_{BG}) for Fe_$Zr_{(pec)}$ was calculated through the Tauc method. (C) Raman spectra (λ = 514 nm) for $Zr_{(pec)}$ – black line, and (B) Fe_$Zr_{(pec)}$ – red line.

Morphologic behavior

SEM images show that citrus pectin has a fibrous morphology (Figure 4A) and that the oxides present a particulate morphology in the form of small granules (Figure 4B and Figure 4C).

The morphology of Fe_Zr$_{(pec)}$ (Figure 4C) does not differ from that of the Zr$_{(pec)}$ (Figure 4B) matrix as expected, which is in agreement with the Raman and XRD data. Qualitative chemical analysis by energy dispersive spectroscopy allowed us to calculate the amount of incorporated iron, from which a value of 11% was found.

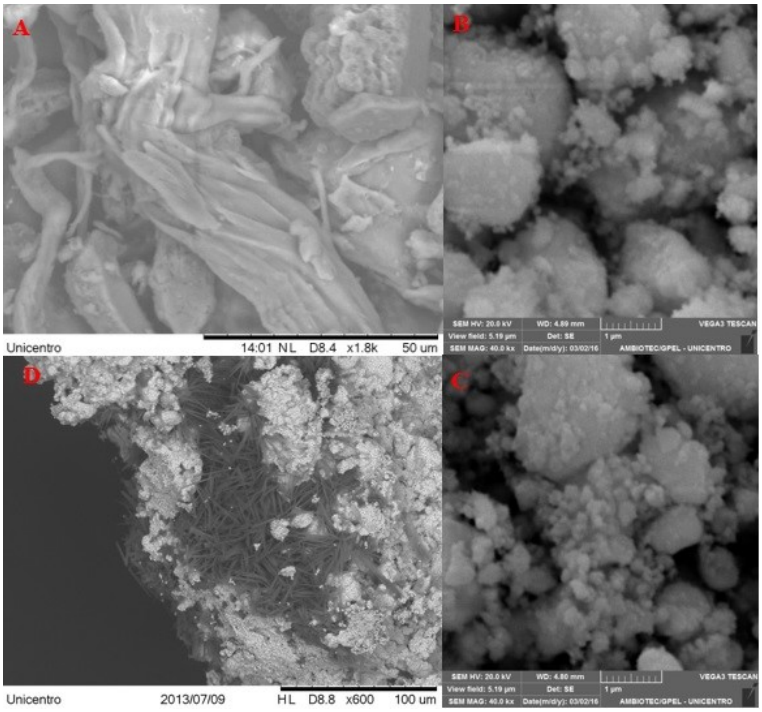


Figure 4. SEM images of: (A) Citrus pectin (B) Zr$_{(pec)}$ (C) Fe_Zr$_{(pec)}$ (D) Fe_Zr$_{(pec)}$ final residue of thermal analysis.

Analysis of the final residue of Fe_Zr$_{(pec)}$ through thermal analysis and SEM (Figure 4D) images shows that the morphology has the appearance of small spheres, differing, therefore, from the initial morphology (Figure 4C). This confirmed the claim that temperature is in fact a key factor for obtaining distinct morphologies and consequently different crystalline phases. However, the formation of a morphology referred to as needles was also observed. These are, according to the literature, hexahedral nanodisks [30].

The Brunauer–Emmett–Teller (BET) method was used to assess the textural properties of the Fe_Zr$_{(pec)}$ sample. The following values were obtained: pore volume = 5.37 × 10^{-2} cm^3 g^{-1}, pore size = 46.30 Å, specific surface area = 23.21 m^2 g^{-1}, and particle size = 391.0 ± 3.8 nm. These values are consistent with a mesoporous material for which the pore size is in the 20–500 Å range according to the International Union of Pure and Applied Chemistry (IUPAC). Studies carried out by Costa and co-workers [31] indicated that some parameters, such as the surface area, pore volume, and pore size, increase with increasing polysaccharide sucrose concentration. This phenomenon, in turn, leads to a change in the oxide matrix with the use of citrus pectin as a gelling agent.

Analysis of the adsorption isotherms and pore distributions shows that the isotherm is type V according to the Brunauer classification, which characterizes materials with macro and mesopores. Type V isotherms are unusual and may appear with certain porous adsorbents, being related to type III isotherms.

Studies on dye degradation

In this work, the binary oxide Fe_Zr$_{(pec)}$ was used to demonstrate its catalytic efficiency relative to other oxides commonly used [32, 33], with the aim of understanding its photocatalytic nature through a Fenton-like process. Zirconia is widely used in catalysis, and it has become a promising candidate for this process in the presence of iron.

Fe_Zr$_{(pec)}$ oxide was active after pH correction of the dye solution used. The incorporation of iron into the zirconia matrix adds photocatalytic properties in the visible (400–800 nm) radiation range. Initially, the variables that may influence the process were investigated, namely, the amount of catalyst and the concentration of H_2O_2. From the performed factorial design, the parameters depicted in Table 1 were optimized.

As seen in Table 1, test 1 showed the highest percentage of dye degradation (47.31%), offering the optimal conditions for the Fenton-like reaction. The amount that each individual or combined factor played in the Fenton-like degradation process was estimated. The factors in this study are positive for the two variables, which means that the increase of both the amount of the sample and the concentration of peroxide led to higher degradation rates.

Table 1. Factorial design 2^2 for optimization of the photo-Fenton process (Reactive Blue dye 4, 50 mg L^{-1}), time of reaction = 10 min.

Variables		**Level (-)**	**Level (+)**
A: **Material amount** (g)		0.015	0.030
B: [H_2O_2] (mg L^{-1})		70	100
	Factor		
Trial	**Catalyst Amount** (mg)	[H_2O_2] (mg L^{-1})	% Degradation
1	30 (+)	100 (+)	47.31 ± 0.92
2	30 (+)	70 (-)	29.92 ± 1.20
3	15 (-)	100 (+)	27.53 ± 0.69
4	15 (-)	70 (-)	25.74 ± 0.75

Main effects: A: 23.96; B: 19.18; A+B: 15.6.

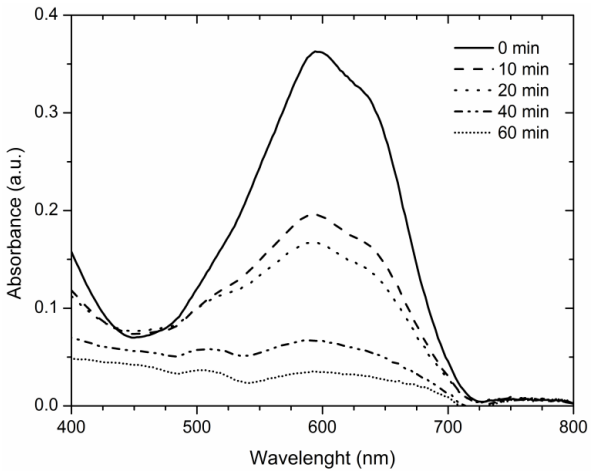


Figure 5. Spectroscopic monitoring of the degradation of reactive blue dye 4 (RB4). Conditions: RB4 - 50 mL at 50 mg L^{-1}, pH 3, mass of the catalyst (Fe_Zr$_{(pec)}$) 30 mg, and 100 mg L^{-1} of H_2O_2 (42% v/v). According to Test 1 highlighted in **Table 1**.

The increase in the H_2O_2 concentration did not induce the same effect, meaning that the main factor in this case was the amount of catalyst. Increasing the amount of catalyst resulted in a 23.96% increase in the degradation efficiency. In contrast, the increase in the H_2O_2 concentration led to a 19.18% increase in degradation. The characteristic band of Reactive Blue dye 4 (599 nm) showed a significant decrease in intensity after 40 min of reaction a large decrease in the chromophore group was observed through spectroscopic monitoring (Figure 5) when the experiment was performed at optimal conditions. After 60 min of reaction, the total degradation of the dye was 90.37%, indicating the elimination of aromatic compounds.

The monitoring of soluble iron (Fe^{2+}/Fe^{3+}) is required as current legislation imposes limits on the amount of iron in wastewater. According to the Federal Conama Resolution number 357 of 17/03/2005, the accepted iron limit is 15 mg L^{-1}. In the performed trials, there was no release of iron ions to the solution, consistent with XRD and Raman data. The Raman data indicated that the iron was in the crystal structure of zirconia as no isolated phases corresponding to iron oxides were observed. The quantification of H_2O_2 is extremely important. In general, the percentage of degradation increases with the increase in the hydrogen peroxide concentration, which is directly

related to the generation of HO• radicals. The monitoring of hydrogen peroxide during the reaction showed that after 60 minutes of reaction it was completely consumed, showing that the amount used (100mg.L^{-1}) was enough for the generation of HO• radicals. In this study, H_2O_2 total consumption was 11 ppm.

The evaluation of the rate constant and half-life time allowed for a quantitative assessment of the Fenton-like process. This photocatalytic degradation process obeyed the Langmuir-Hinshelwood kinetic expression, $\ln(C/C_0) = -kt$, wherein C and C_0 correspond to initial and final concentrations of the dye model, respectively; k at constant speed and t the treatment time, following a pseudo-first-order kinetic with respect to the disappearance of the substrate of interest [34]. The absorptivity of the dye was 0.0072 L mg^{-1} cm^{-1}. The reaction order was checked through the graph method, a rate constant of 0.0368 min^{-1} and a half-life time of 18.83 min were calculated from the Lambert–Beer equation [35].

3. Material and Methods

Reagents

Zirconium nitrate ($ZrO(NO_3)_2$•$5H_2O$) and Iron nitrate ($Fe(NO_3)_3$•$9H_2O$) (Vetec) was employed. Reactive Blue 19 dye (C.I. 61200, Sigma-Aldrich) was used in 50 mg.L^{-1} aqueous solution. Hydrogen peroxide (H_2O_2, Nuclear, 10% m/m) and ferrous chloride ($FeCl_3$, Merck). All chemicals were analytical grade and used as received without further purification. Deionized water was used throughout experiments.

Synthesis of $Zr_{(pec)}$ and $Fe_Zr_{(pec)}$ oxides

Zirconium nitrate [$ZrO(NO_3)_2$•$5H_2O$, 0.20 mol L^{-1}] was added to an aqueous solution of citrus pectin (1.00% by mass, Vetec) under constant stirring and controlled heating (80 °C). The complete gelling of the solution occurred over a 3-h period [36]. The gel was calcined in a muffle furnace at 600 °C. The calcination temperature was determined from the thermal analysis curve previously obtained for the citrus pectin gel. The solid was then macerated and named $Zr_{(pec)}$. The iron zirconate was prepared following the same route of synthesis as $Zr_{(pec)}$. Iron nitrate [$Fe(NO_3)_3$•$9H_2O$, 0.03 mol L^{-1}] and zirconium nitrate (0.02 mol L^{-1}) aqueous solutions were prepared. The solutions were added to the pectin solution (1.00% by mass) at the same time. The resulting solution was maintained under heating (80 °C) and constant stirring for 3 h. The gel was calcined in the muffle (600 °C) and the solid was named $Fe_Zr_{(pec)}$.

Photo-Fenton process and analytical control

The photo-Fenton process was performed in a bench photochemical reactor [37-39] equipped with a water-cooling system, mechanical agitation, and temperature control (25 °C). The radiation source was a 125 W mercury vapor lamp (no bulb shield), which was inserted into the solution by means of a Pyrex glass bulb. In the degradation experiments, a Reactive Blue R19 dye solution (RB19, 50 mL at 50 mg L^{-1}, pH 3) was used, along with a mass of 15–30 mg of iron zirconate and pre-defined quantities of H_2O_2 (42% v/v).

During the photo-Fenton process, solution aliquots were collected with a syringe (10 mL coupled with a filter) directly from the reactor every 10 min for effective analytical control. Residual hydrogen peroxide was determined spectrophotometrically, using the methodology based on the ammonium vanadate reaction [40, 42]. The o-phenanthroline method was used to monitor the leached iron ions of the samples [39, 42]. The spectroscopic monitoring of the degradation of the dyes was performed with a UV-VIS spectrophotometer (Varian 3000) using a quartz cuvette with a 1.0 cm optical path. The percentage of degradation was calculated from the absorbance reduction at the wavelength of maximum absorption of the dye at 599 nm.

Characterization techniques

Thermal analysis curves were obtained using a simultaneous thermogravimetric analyzer, Seiko, TG/DTA model 6300, at a heating rate of 15 ^oC min^{-1} from 30 ^oC to 1200 ^oC in a platinum pan (sample holder) with a dynamic atmosphere of compressed air at a flow rate of 300 mL min^{-1}. X-ray difractometry (XRD) using a Bruker D2 Phaser diffractometer equipped with a LynxEye detector and copper ($\lambda_{K\alpha}$ = 1.54 Å) radiation source. Electronic spectra were obtained by

diffuse reflectance with an Ocean Optics USB 2000 fiber optic spectrophotometer. Raman spectra were obtained with a Bruker Senterra microscope using a green laser (λ = 514 nm). SEM images were obtained with a Hitachi High-Tech TM3000 microscope coupled to a SwiftED3000. The samples specific surface areas were calculated by the multi-point Brunauer–Emmett–Teller (BET) method, performed with a NOVA-2000 Quantachrome. The samples were pre-treated through heating at 180 °C for 2 h under vacuum.

4. Conclusions

The present results indicate the feasibility of the proposed method for obtaining zirconium oxide and mixed zirconium oxide of iron from citrus pectin and nitrates through an environmentally friendly route as the solvent used is water and the precursor is a polysaccharide. The synthesis proved promising not only for obtaining zirconium oxide but also for obtaining other oxides.

The oxides were thermally stable and with similar compositions. The XRD data showed that there was a decrease of both the crystallinity and the crystallite size. The electronic spectra showed differences attributed to iron embedded in the zirconia matrix. The application of Fe_Zr(pec) in the degradation of dyes was shown to be suitable for a Fenton-like process, promoting efficient bleaching of the dye solution over 40 min

Acknowledgments

The authors would like to thank the Capes Agency (Nos. 028/2009 and 063/2010), Fundação Araucária, CNPq (Scholarship Researcher No. 305447/2013-0 and Grant No. 447902/2014-8), and FINEP (Nos. 01.09.0393.00 and 01.12.0471.00). C. Antoniazzi acknowledge a DS-Capes research scholarship.

References and Notes

[1] Pakma, O.; Ozdemir, C.; Kariper, A.; Ozaydin, C.; Gddotulddotu, O. *Appl. Surf. Sci.* **2016,** *377*, 159. [Crossref]

[2] Guo-liang, S.; Feng, Y.; Xiao-liang, Y.; Rui-feng, L. *Fuel Chem Technol.* **2017,** *45*, 311. [Crossref]

[3] Manjunatha, S.; Dharmaprakash, M.S. *J. Lumin.* **2016,** *180*, 20. [Crossref]

[4] Reddy, Ch. V.; Babu, B.; Reddy, I. N.; Shim, J. *Ceram. Int.* **2018,** *44,* 6940. [Crossref]

[5] Kwon, O. H.; Jang, C.; Lee, J.; Jeong, H. Y.; Kwon, Y.; Joo, J. H.; Kim, H. *Ceram. Inter.* **2017,** *43,* 8236. [Crossref]

[6] Alkhayatt, A. H. O.; Hussain, S. A.; Mahdi, E. A. *Optik* **2018,** *159*, 305. [Crossref]

[7] Wang, F.; Xia, W.; Mu, X.; Chen, K.; Si, H.; Li, Z. *Appl. Surf. Sci.* **2018,** *439*, 405. [Crossref]

[8] Singha, R. K.; Shukla, A.; Yadav, A.; Adak, S.; Iqbal, Z.; Siddiqui, N.; Bal, R. *Appl. Energy* **2016,** *178*, 110. [Crossref]

[9] Mekala, R.; Rajendran, V. *Optik* **2017,** *145*, 142. [Crossref]

[10] Gnanamoorthi, K.; Balakrishnan, M.; Mariappan, R.; Kumar, E. R. *Mater. Sci. Semicond. Process* **2015,** *30*, 518. [Crossref]

[11] Kennedy, K.; Stefansky, T.; Davy, G.; Zackay, V. F.; Parker, E. R. *J. Appl. Phys.* **1965,** *36,* 3808. [Crossref]

[12] Mierczyńska, J.; Cybulska, J.; Zdunek, A. *Carbohydr. Polym.* **2017,** *156*, 443. [Crossref]

[13] Xu, S. Y.; Liu, J. P.; Huang, X.; Du, L. P.; Shi, F. L.; Dong, R.; Huang, X. T.; Zheng, K.; Liu, Y.; Cheong, K. L. *LWT* **2018,** *90*, 577. [Crossref]

[14] Ho, G. T. T.; Ahmed, A.; Zou, Y. F.; Aslaksen, T.; Wangensteen, H.; Barsett, H. *Carbohydr. Polym.* **2015,** *125*, 314. [Crossref]

[15] Popov, S. V.; Ovodova, R. G.; Golovchenko, V. V.; Khramova, D. S.; Markov, P. A.; Smirnov, V. V.; Shashkov, A. S.; Ovodov, Y. S. *Food Chem.* **2014,** *143*, 106.

[16] Antoci, A.; Galeotti, M.; Sordi, S. *Commun. Nonlinear Sci. Numer. Simul*. **2018,** *58*, 262. [Crossref]

[17] Nimkar, U. *Curr. Opin. Green Sustainable Chem.* **2018,** *9*, 13. [Crossref]

[18] Lomax, S. Q.; Lomax, J. F.; Graham, T. K.; Moore, T. J. T.; Knapp, C. G. *J. Cult. Heritage* **2018.** [Crossref]

[19] Walling, C. *Acc. Chem. Res.* **1975,** *8* ,125. [Crossref]

[20] Pignatello, J. J.; Oliveros, E.; MacKay, A. *Crit Rev Environ Sci Technol.* **2006,** *36* 1. [Crossref]

[21] Shao, G. N.; Imran, S. M.; Jeon, S. J.; Engole, M.; Abbas, N.; Haider, M. S.; Kang, S. J.; Kim, H. T. *Powder Technol.* **2014,** *258,* 99. [Crossref]

[22] Sherman, D. M.; Waite, T. D. *Am. Mineral.* **1985,** *70,* 1262. [Link]

[23] Davar, M. A. F. *J. Mol. Liq.* **2016**, *221*, 1071. [Crossref]

[24] Shao, G. N.; Elineema, G.; Quang, D. V.; Kim, Y. N.; Shim, Y. H.; Hilonga, A.; Kim, J.-K.; Kim, H. T. *Powder Technol.* **2012,** *217,* 489. [Crossref]

[25] Štefanić, G.; Musić, S.; Popović, S.; Sekulić, A. *J. Mol. Struct.***1997,** *408/409*, 391. [Crossref]

[26] Lide, D. R. Handbook of Chemistry and Physics, Nova York: CRC, 2004.

[27] Tauc, J. *Mater. Res. Bull.***1968,** *3,* 37. [Link]

[28] Naumenko, A.; Gnatiuk, I.; Smirnova, N.; Eremenko, A. *Thin Solid Films* **2012,** *520,* 4541. [Crossref]

[29] Muller, M.; Villalba, J. C. Mariani, F. Q.; Dalpasquale, M.; Lemos, M. L.; Anaissi, F. J. *Dyes Pigm.* **2015,** *120,* 271. [Crossref]

[30] Kumari, L.; Du, G. H.; Li, W. Z.; Vennila, R. S.; Saxena, S. K.; Wang, D. Z. *Ceram. Int.* **2009,** *35,* 2401. [Crossref]

[31] da Costa, J. C. D.; Coombs, S.; Lim, J. et al. *J. Sol-Gel Sci. Technol.* **2004**, *31*, 215. [Crossref]

[32] Shao, G. N.; Hilonga, A.; Jeon, S. J.; Lee, J. E.; Elineema, G.; Quang, D. V.; Kim, J.-K.; Kim, H. T. *Powder Technol.* **2013,** *233,* 123. [Crossref]

[33] Benjume, M. L. G.; Cabrera, M. I. E.; Garcia, M. E. C. *Int. J. Photoenergy* **2012,** *2012,* 10. [Crossref]

[34] Muruganandham, M.; Swaminathan, M. *Sep. Purif. Technol.* **2006,** *8*, 297. [Crossref]

[35] Haji, S.; Benstaali, B.; Al-Bastaki, N. *Chem. Eng. J.* **2011,** *168*, 134. [Crossref]

[36] Dalpasquale, M.; Mariani, F. Q.; Muller, M.; Anaissi, F. J. *Dyes Pigm.* **2016,** *125,* 124. [Crossref]

[37] Anaissi, F. J.; Villalba, J. C.; Fujiwara, S. T.; Cotica, L. F.; Zamora-Peralta, P.; Souza, C. R. L. *Quim. Nova,* **2009,** *32,* 2006. [Crossref]

[38] Leao Neto, V. S.; Orcelli, T.; Silva, M. R.; Anaissi, F. J.; Urbano, A.; Takashima, K. *React. Kinet. Mech. Cat.* **2016,** *117,*815. [Crossref]

[39] Ribeiro, K.; Andrade, T. M. Fujiwara, S. T. *Environ. Technol.* **2016,** *37,* 1664. [Crossref]

[40] Oliveira, M. C.; Nogueira, R. F. P.; Gomes Neto, J. A.; Jardim, W. F.; Rohwedder, J. J.R. *Quim. Nova* **2001,** *24*, 188. [Link]

[41] Nogueira, R. F. P.; Oliveira, M. C.; Paterlini, W. C. *Talanta* **2005,** *66*, 86. [Crossref]

[42] APHA - American Public health Association, Standard Methods for Examination of Water and Wastewater, nineteenth edition, American Public Health Association - American Water Works Associations, Washington. 1998. [Link]